ESEEM Studies of Alcohol Binding to the Manganese Cluster of the Oxygen Evolving Complex of Photosystem II

Dee Ann Force, David W. Randall,† Gary A. Lorigan,‡ Keri L. Clemens, and R. David Britt*

Contribution from the Department of Chemistry, University of California, Davis, California 95616-0935

Received July 30, 1998. Revised Manuscript Received October 16, 1998

Abstract: An ESEEM (electron spin−echo envelope modulation) spectroscopic study employing a series of ^{2}H-labeled alcohols provides direct evidence that small alcohols (methanol and ethanol) ligate to the Mn cluster of the oxygen evolving complex (OEC) of Photosystem II in the S_2-state of the Kok cycle. A numerical method for calculating the through-space hyperfine interactions for exchange-coupled tetranuclear Mn clusters is described. This method is used to calculate hyperfine interaction tensors for protons [deuterons] in the vicinity of two different arrangements of Mn ions in a tetranuclear cluster: a symmetric cubane model and the EXAFS-based Berkeley "dimer-of-dimers" model. The Mn−H distances derived from the spectroscopically observed coupling constants for methanol and ethanol protons [deuterons] and interpreted with these cluster models are consistent with the direct ligation of these small alcohols to the OEC Mn cluster. Specifically, for methanol we can simulate the three-pulse ESEEM time domain pattern with three dipolar hyperfine interactions of 2.92, 1.33, and 1.15 MHz, corresponding to a range of maximal Mn−H distances in the models of 3.7−5.6 Å (dimer-of-dimers) and 3.6−4.9 Å (symmetric cubane). We also find evidence for limited access of *n*-propanol, but no evidence for 2-propanol or DMSO access. Implications for substrate accessibility to the OEC are discussed.

Introduction

Molecular oxygen is produced by plants and cyanobacteria as an incidental byproduct of the water-splitting reaction performed by the oxygen evolving complex (OEC) of membrane-bound Photosystem II (PSII). During electron transport coupled to the oxidation of water, a transmembrane proton gradient is generated which is ultimately utilized to synthesize ATP. The OEC consists of a tetranuclear manganese cluster, the redox-active tyrosine Y_Z (D1-Tyr161, *Synechocystis* numbering), and essential cofactors Ca^{2+} and Cl^-. Four photoinduced oxidizing equivalents are accumulated by the OEC; this process is advanced stepwise through a series of S-states ($S_{n=0-4}$) and culminates in the release of O_2, resetting the cycle to the most reduced state, S_0.[1] The precise mechanism of the water oxidation, as well as the complete details of OEC structure and ligation, remain elusive despite intense study (for reviews, see refs 2−5). Recent models postulate a metalloradical mechanism: Mn oxidation occurs concomitantly with proton[2,6] or hydrogen atom[7−9] abstraction from coordinated water/hydroxide ligands by the photo-oxidized $Y_Z^{\bullet}$ neutral radical. In these models, $Y_Z^{\bullet}$ is directly involved in the water-splitting chemistry, in addition to its long-characterized role as a fast electron-transfer agent between the OEC and the primary photo-oxidation product, the chlorophyll cation P_{680}^+. However, such models remain controversial.[10]

The S_2-state of the Kok cycle is EPR (electron paramagnetic resonance) active and produces two types of CW-EPR (continuous wave EPR) signal: the $g = 2$ "multiline" signal (MLS)[11] and the $g = 4.1$ signal.[12,13] The S_2-state MLS arises from a ground spin state $S = {}^1/_2$ of an antiferromagnetically exchange-coupled Mn cluster;[14−16] the $g = 4.1$ signal is thought to arise from a higher spin state such as $S = {}^3/_2$ or $S = {}^5/_2$.[17−20] The

† Present address: Department of Chemistry, Stanford University, Stanford, CA 94305.

‡ Present address: Department of Chemistry and Biochemistry, Miami University, Oxford, OH 45056.

(1) Kok, B.; Forbush, B.; McGloin, P. *Photochem. Photobiol.* **1970**, *11*, 457−475.

(2) Britt, R. D. In *Oxygenic Photosynthesis: The Light Reactions*; Ort, D. R., Yocum, C. F., Eds.; Kluwer Academic: Dordrecht, The Netherlands, 1996; pp 137−164.

(3) Yachandra, V. K.; Sauer, K.; Klein, M. P. *Chem. Rev.* **1996**, *96*, 2927−2950.

(4) Debus, R. J. *Biochim. Biophys. Acta* **1992**, *1102*, 269−352.

(5) Rutherford, A. W.; Zimmermann, J.-L.; Boussac, A. In *The Photosystems: Structure, Function, and Molecular Biology*; Barber, J., Ed.; Elsevier: Amsterdam, 1992; pp 179−229.

(6) Gilchrist, M. L.; Ball, J. A.; Randall, D. W.; Britt, R. D. *Proc. Natl. Acad. Sci. U.S.A.* **1995**, *92*, 9545−9549.

(7) Tommos, C.; Tang, X.-S.; Warncke, K.; Hoganson, C. W.; Styring, S.; McCracken, J.; Diner, B. A.; Babcock, G. T. *J. Am. Chem. Soc.* **1995**, *117*, 10325−10335.

(8) Hoganson, C. W.; Lyadkis-Simantiris, N.; Tang, X.-S.; Tommos, C.; Warncke, K.; Babcock, G. T.; Diner, B. A.; McCracken, J.; Styring, S. *Photosyn. Res.* **1995**, *46*, 177−184.

(9) Hoganson, C. W.; Babcock, G. T. *Science* **1997**, *277*, 1953−1956.

(10) Ahlbrink, R.; Haumann, M.; Cherepanov, D.; Bögershausen, O.; Mulkidjanian, A.; Junge, W. *Biochemistry* **1998**, *37*, 1131−1142.

(11) Dismukes, G. C.; Siderer, Y. *FEBS Lett.* **1980**, *121*, 78−80.

(12) Casey, J. L.; Sauer, K. *Biochim. Biophys. Acta* **1984**, *767*, 21−28.

(13) Zimmermann, J.-L.; Rutherford, A. W. *Biochim. Biophys. Acta* **1984**, *767*, 160−167.

(14) Britt, R. D.; Lorigan, G. A.; Sauer, K.; Klein, M. P.; Zimmermann, J. L. *Biochim. Biophys. Acta* **1992**, *1140*, 95−101.

(15) Lorigan, G. A.; Britt, R. D. *Biochemistry* **1994**, *33*, 12072−12076.

(16) Hansson, Ö.; Aasa, R.; Vänngård, T. *Biophys. J.* **1987**, *51*, 825−832.

(17) Astashkin, A. V.; Kodera, Y.; Kawamori, A. *J. Magn. Res. Ser. B* **1994**, *105*, 113−119.

(18) Haddy, A.; Dunham, W. R.; Sands, R. H.; Aasa, R. *Biochim. Biophys. Acta* **1992**, *1099*, 25−34.

(19) Zimmermann, J.-L.; Rutherford, A. W. Biochemistry **1986**, *25*, 4609−4615.

10.1021/ja982713b CCC: $15.00
Published on Web 12/30/1998

MLS exhibits 16−19 lines of partially resolved hyperfine structure over the 1500 G wide spectrum. The $g = 4.1$ signal may range from 300 to 400 G wide (measured peak to trough), depending upon sample treatment,[4] and is featureless for unoriented membrane samples, although oriented preparations treated with ammonia display ^{55}Mn hyperfine structure.[21,22] It has been reported that the state responsible for the MLS is reversibly converted to the $g = 4.1$ signal state when near-IR light is absorbed during illumination at 150 K; the MLS reappears if illumination is followed by dark-annealing at 200 K.[23] This transformation does not occur if the illumination and subsequent dark-incubation steps are performed at 200 K.[24]

It has been known for some time that various alcohols enhance the amplitude of the MLS at the expense of the $g = 4.1$ signal. The formation of the $g = 4.1$ signal is inhibited by 4% ethanol in the presence of sucrose, 30% ethylene glycol, or 50% glycerol.[19] The signal is reported to be eliminated by 3% methanol in the presence of sucrose.[25] These same alcohols are reportedly found to elicit better resolution in the ^{55}Mn hyperfine (hf) splitting pattern of the MLS compared to protein without added alcohol.[19,24,25] Observation of a multiline EPR signal from the S_0 state, undetected until recently, requires the presence of 0.5−1.5% methanol[26,27] (3% methanol[28]); 5% ethanol does *not* have a similar effect.[26] Frash et al.[29] examined PSII reaction center preparations lacking the 17 and 23 kDa extrinsic proteins and presented evidence that glycerol, propargyl alcohol, and ethanol can be oxidized to aldehydes by the OEC in the presence of peroxide. No native OEC alcohol reactivity has been reported.

Such empirical evidence suggests that small alcohols may bind in close proximity to the Mn cluster and thus could be useful as molecular probes of the OEC ligation sphere, and possibly as analogs for substrate water. A particular benefit in using these alcohols in an isotope-sensitive magnetic resonance experiment is the nonexchangeability of all but the alcoholic (OH) proton. Unlike the situation for deuterated water, whose deuterons can freely exchange with an indeterminate number of amino acid functionalities and thus make isolation of the deuteron signature of the originally labeled water molecules quite difficult,[30] one may precisely identify the binding of such ^{2}H-labeled alcohols into sites that are in proximity to the paramagnetic center of interest, in this case the Mn cluster.

This work exploits this advantage by investigating the accessibility of small alcohols to the OEC using three-pulse ESEEM (electron spin−echo envelope modulation) spectroscopy. The immediate environment of the Mn cluster is directly probed in PSII membranes treated with a series of natural abundance and ^{2}H-labeled alcohols which range in size and bulkiness in order to determine the spatial milieu of the active site as well as its binding characteristics.

Materials and Methods

Materials. Phenyl-*p*-benzoquinone (PPBQ) was obtained from Aldrich and recrystallized from ethanol. The ^2H_2O (99.96% deuterium enrichment; low paramagnetic), deuterated alcohols (≥99% deuterium enrichment: methanol-d_3, methanol-d_4, ethanol-d_6, 2-propanol-d_8, and *n*-propanol-d_7), and DMSO-d_6 (99.9% deuterium enrichment) were used as received from Cambridge Isotope Laboratories. Ethanol (dehydrated, USP punctilious) was used as received from Quantum Chemical. All other chemicals were used as received from Fisher Scientific.

Sample Preparation. PSII-enriched membranes were isolated from commercial spinach using a method based upon that of Berthold et al.[22,31,32] The PSII membranes were washed in a buffer containing 400 mM sucrose/50 mM MES−NaOH (pH 6.0)/5 mM $MgCl_2$/15 mM NaCl/5 mM $CaCl_2$/1 mM EDTA (SMNCE buffer) at 1 mg of chlorophyll (Chl)/mL; after removal of aliquots for oxygen evolution, the samples were centrifuged for 30 min at 40 000*g*. The pelleted membranes were then resuspended in SMNCE buffer and loaded into 3.8 mm o.d. precision quartz EPR tubes at concentrations of 15−20 mg of Chl/mL, corresponding to maximum PSII concentrations of approximately 100 μM.

The alcohol, ^2H_2O, and DMSO-treated samples were obtained by using an SMNCE wash and resuspension buffer which contained the desired concentration of alcohol, ^2H_2O, or DMSO; the SMNCE buffer made with 55 M ^2H_2O was adjusted to pD 6.0; all others were pH 6.0. Samples used for annealing studies had 1 mM PPBQ (final concentration; from a 200 mM stock solution in DMSO) added to the resuspension buffer. Uncryoprotected alcohol-treated and control samples were prepared in buffers without sucrose, though otherwise in an analogous fashion. Following dark-adaptation on ice for 30−45 min, the EPR samples were stored at 77 K. Oxygen-evolution rates obtained for control PSII samples typically were 450−550 μmol of O_2/mg of Chl per hour. Chlorophyll determination was done according to Arnon.[33]

Determination of Comparative O_2 Evolution Rates. The O_2 evolution measurements used to compare the relative effects of the addition of alcohols were as follows: O_2 evolution measurements were performed at 25 °C using a YSI 5331 oxygen electrode. The measuring chamber contained 1200 μL of SMNCE buffer with one of the concentration series (1.0, 2.0, 3.5, or 5.0 M) of the alcohols methanol, ethanol, 2-propanol, or *n*-propanol, as well as 10 μL of a stock solution of 200 mM PPBQ in DMSO. An aliquot of the untreated PSII sample containing 10 μg of Chl was added, and the assay mixture was stirred for 5 s in the dark before illumination (Schott 1500L IR-filtered 150 W fiber optic lamp).[34] Oxygen evolution rates were measured as the slope of the straight line between the 5 and 20 s timepoints after the onset of illumination. A minimum of 4 trials per molarity of alcohol were obtained, using samples from a minimum of two separate PSII preparations. Control rates were taken periodically throughout the data collection using a sample assay mixture that did not contain alcohol.

Four additional trials, which used aliquots of PSII washed in 5.0 M methanol-containing SMNCE and then assayed for O_2 evolution activity in an alcohol-free mixture, were also performed in order to check for reversibility of any effects specific to this concentration of methanol. In a similar fashion, a single PSII preparation was divided and each portion washed in an SMNCE buffer containing 3.5 M of either ethanol, 2-propanol, or *n*-propanol, as well as the alcohol-free control, and then

(20) dePaula, J. C.; Beck, W. F.; Brudvig, G. W. *J. Am. Chem. Soc.* **1986**, *108*, 4002−4009.
(21) Kim, D. H.; Britt, R. D.; Klein, M. P.; Sauer, K. *J. Am. Chem. Soc.* **1990**, *112*, 9389−9391.
(22) Kim, D. H.; Britt, R. D.; Klein, M. P.; Sauer, K. *Biochemistry* **1992**, *31*, 541−547.
(23) Boussac, A.; Girerd, J.-J.; Rutherford, A. W. *Biochemistry* **1996**, *35*, 6984−6989.
(24) dePaula, J. C.; Beck, W. F.; Miller, A. F.; Wilson, R. B.; Brudvig, G. W. *J. Chem. Soc., Faraday Trans.* **1987**, *83*, 3635−3651.
(25) Pace, R. J.; Smith, P.; Bramley, R.; Stehlik, D. *Biochim. Biophys. Acta* **1991**, *1058*, 161−170.
(26) Messinger, J.; Nugent, J. H. A.; Evans, M. C. W. *Biochemistry* **1997**, *36*, 11055−11060.
(27) Messinger, J.; Robblee, J. H.; Yu, W. O.; Sauer, K.; Yachandra, V. K.; Klein, M. P. *J. Am. Chem. Soc.* **1997**, *119*, 11349−11350.
(28) Åhrling, K. A.; Peterson, S.; Styring, S. *Biochemistry* **1997**, *36*, 13148−13152.
(29) Frasch, W. D.; Mei, R.; Sanders, M. A. *Biochemistry* **1988**, *27*, 3715−3719.
(30) Gilchrist, M. L.; Force, D. A.; Randall, D. W.; Peloquin, J. M.; Ball, J. A.; Britt, R. D. Manuscript in preparation.
(31) Berthold, D. A.; Babcock, G. T.; Yocum, C. F. *FEBS Lett.* **1981**, *134*, 231−234.
(32) Ford, R. C.; Evans, M. C. W. *FEBS Lett.* **1983**, *160*, 159−164.
(33) Arnon, D. I. *Plant Physiol.* **1949**, *24*, 1−14.
(34) Several initial trials (data not shown) showed no significant difference in O_2 evolution rate whether the PSII sample was washed in an alcohol-containing or alcohol-free buffer prior to the rate determination performed in an alcohol-containing assay mixture. Using a sample washed in an alcohol-free buffer allowed using the same stock solution of sample for the O_2 evolution measurements and reduced the inherent uncertainty of making numerous Chl determinations as well as using sample aliquots of differing volume for each alcohol trial.

assayed twice in a mixture identical to the wash buffer as well as in an alcohol-free buffer solution.

EPR Spectroscopy. CW-EPR spectra were collected at a temperature of 7.0 K with a Bruker ECS106 X-band CW-EPR spectrometer equipped with an Oxford ESR900 liquid helium cryostat and ITC503 gas flow and temperature controller. All of the CW-EPR experiments were obtained under the following conditions: 9.50 GHz microwave frequency; 100 kHz modulation frequency; 5 mW microwave power and 16 G modulation amplitude (MLS and $g = 4.1$ spectra); 80 μW microwave power and 1.6 G modulation amplitude ($Y_D^{\bullet}$ spectra). Both the MLS and $g = 4.1$ spectra were obtained at microwave powers well below saturating conditions at this temperature. Calculations for the relative amounts of $g = 4.1$ signal were made by first scaling each S_2-state spectrum to the amplitude of $Y_D^{\bullet}$, then normalizing the largest $g = 4.1$ peak-to-trough measurement to 100, and scaling the other $g = 4.1$ amplitudes accordingly, yielding relative percentages. The MLS calculations were performed in analogous fashion by summing the second through sixth peaks below $g = 2$, marked with asterisks in Figure 2. ESEEM spectra were collected at a temperature of 4.2 K on a laboratory-built pulsed EPR spectrometer.[35] All of the three-pulse ($\pi/2-\tau-\pi/2-T-\pi/2-\tau-ESE$) ESEEM experiments were obtained under the following conditions: $\pi/2$ pulse width 15 ns; τ 219 ns; repetition rate 200 Hz; microwave frequency 9.26582 GHz; magnetic field 3220 G. The τ value was chosen as an integer multiple of the proton Larmor period in order to suppress the weakly coupled proton modulations while at the same time maximizing the contribution from any deuterons; this τ value is also approximately one-half of the deuteron Larmor period. The field position is 50 G downfield from the large $Y_D^{\bullet}$ radical signal at $g = 2$. A cosine Fourier backfill was used to reconstruct the instrumental dead time.[36]

For $S_1 \rightarrow S_2$ advancement, samples were illuminated at 200 K (dry ice/methanol) in a half-silvered dewar using a focused 300 W IR-filtered Radiac lamp for 5 min. Sample annealing was done at 4 °C (ice/water) in total darkness for 1 min followed by freezing to 77 K.

Computer simulations of the ESEEM data were based on the density matrix formalism of Mims[37,38] using the numerical algorithm described by Britt et al.[39] The nuclear quadrupole parameters used for deuterium in the simulations, $\eta = 0.1$ and $e^2Qq = 0.22$ MHz, were those used in the ESEEM characterization of water and methanol ligation to a mixed valence dinuclear Mn complex.[40] A numerical method[41] for calculating proton dipolar hyperfine interactions for an exchange-coupled tetranuclear Mn cluster was employed using different geometric models for the OEC. Three-dimensional interpolated dipolar hyperfine isosurfaces were produced by the DataExplorer computer graphics program.[42]

Results

Relative Oxygen Evolution Rates. The oxygen evolution rates were measured for PSII samples treated with varying concentrations of methanol, ethanol, 2-propanol, or *n*-propanol. These measurements show that all 1.0 M alcohol-treated PSII samples have undiminished rates compared to the untreated control. However, as displayed in Figure 1, at higher concentrations the four alcohol treatments used in this study show different concentration-dependent effects on the oxygen evolving rate. For alcohol treatment concentrations higher than 1.0 M, the decline in oxygen evolution rates varied from minor (methanol) to severe (2-propanol and *n*-propanol). The 14% reduction in oxygen evolution activity by 5.0 M methanol treatment was found to be fully reversible; normal activity was restored by subsequently assaying the 5.0 M methanol-exposed sample in an alcohol-free solution (data not shown). The trials comparing the reversibility of the 3.5 M alcohol inhibitions (i.e., samples washed in alcohol-containing buffer, followed by the assay of individual portions for oxygen evolution in alcohol-containing or alcohol-free solution) are as follows (data not shown): the 3.5 M ethanol-washed PSII samples recovered to slightly greater than the control rate; the 3.5 M 2-propanol- and *n*-propanol-washed samples recovered to ~75 and ~12% of the control rate, respectively. We observe that the proteins are not irreversibly damaged at the alcohol concentrations used in the CW-EPR and ESEEM studies (vide infra).

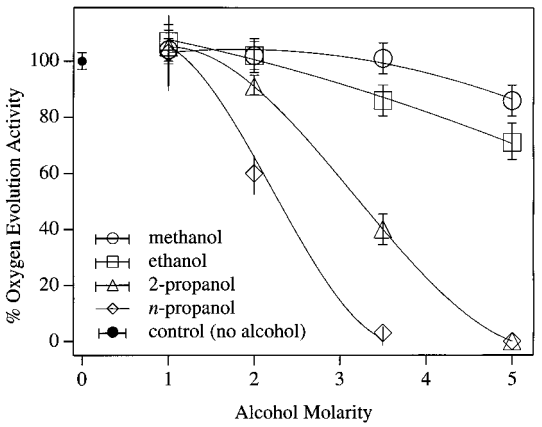

Figure 1. Effect of small alcohols on the light-induced O_2 evolution rates of PSII samples. Rates were normalized to the control rate, which was set to 100%. The control rate is the average of 17 trials from four separate PSII preparations. Other rates are the average of at least four trials, taken from at least two separate PSII preparations. Error bars are the standard deviation for small data sets: $s = \sqrt{(\sum_{i=1}^{N}(x_i-\bar{x})^2)/(N-1)}$. Solid lines are polynomial fits to the data. See Materials and Methods for procedural details.

CW-EPR. The CW-EPR spectra obtained for all alcohol-treated PSII samples poised in the S_2 state show an alcohol concentration dependence on the relative amplitudes of the $g = 4.1$ and the multiline signals. For example, the presence of 100 mM methanol enhances the PSII MLS at the expense of the $g = 4.1$ signal (compare Figure 2a and b); the 1.0 M methanol treatment has an even greater influence, eliminating most of the $g = 4.1$ signal (Figure 2c).[43]

These data were obtained from samples using 400 mM sucrose as a cryoprotectant. Figure 3 shows the effect of 0 and 1.0 M methanol in the absence of sucrose. The $g = 4.1$ signal of the sucrose containing sample (Figure 2a) is enhanced in comparison to the spectrum of a parallel alcohol-free PSII sample without cryoprotectant (Figure 3a). Nonetheless, the 1.0 M methanol treatment reduces the $g = 4.1$ to MLS signal ratio without sucrose as well. These results suggest that the effect of alcohol is independent of the presence of sucrose.

The CW-EPR spectra obtained for ethanol, 2-propanol, and *n*-propanol follow the same trend as methanol-treated PSII.

(35) Sturgeon, B. E.; Britt, R. D. *Rev. Sci. Instrum.* **1992**, *63*, 2187−2192.
(36) Mims, W. B. *J. Magn. Res.* **1984**, *59*, 291−306.
(37) Mims, W. B. In *Electron Paramagnetic Resonance*; Geschwind, S., Ed.; Plenum Press: New York, 1972; pp 263−351.
(38) Mims, W. B. *Phys. Rev. B* **1972**, *5*, 2409−2419.
(39) Britt, R. D.; Zimmermann, J.-L.; Sauer, K.; Klein, M. P. *J. Am. Chem. Soc.* **1989**, *111*, 3522−3532.
(40) Randall, D. W.; Gelasco, A.; Caudle, M. Y.; Pecoraro, V. L.; Britt, R. D. *J. Am. Chem. Soc.* **1997**, *119*, 4481−4491.
(41) Randall, D. W. Ph.D. Dissertation. Department of Chemistry, University of California, Davis, 1997.
(42) International Business Machines, Yorktown Heights, NY, 1996.

(43) Although in this specific group of spectra a small increase in the amount of photooxidized cyt b_{559}, monitored by the $g \approx 3$ peak near 2200 G, was observed with increased methanol, over our multiple sets of spectra no correlation between photooxidized cyt b_{559} and alcohol type or molarity (100 mM or 1.0 M) was detected. Furthermore, we observed no correlation between alcohol type or molarity and the amplitude of the $Y_D^{\bullet}$ tyrosine signal over this range of concentrations where the OEC remains fully functional (Figure 1).

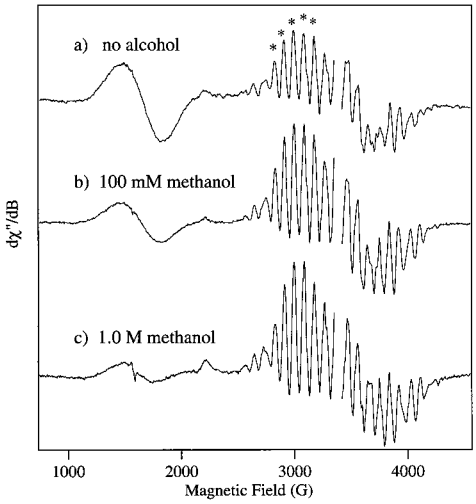

Figure 2. CW-EPR spectra of the S_2-state Mn signals from PSII samples containing: (a) 0 M (control), (b) 100 mM, or (c) 1.0 M methanol in cryoprotected buffer (400 mM sucrose). Background spectra obtained before illumination have been subtracted and the large $Y_D^{\bullet}$ tyrosine radical signal centered at $g = 2$ has been removed for clarity. The features marked by asterisks were summed to quantify the MLS intensity. Instrument parameters: temperature, 7.0 K; microwave frequency, 9.50 GHz; microwave power, 5 mW; modulation amplitude, 16 G; modulation frequency, 100 kHz.

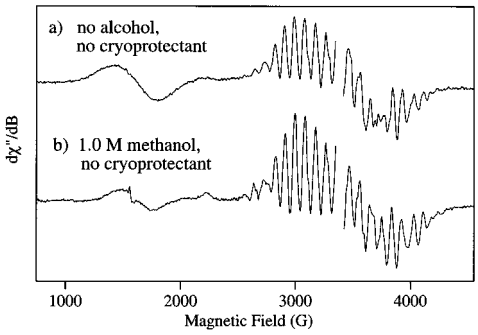

Figure 3. CW-EPR spectra of the S_2-state Mn signals from PSII samples containing: (a) 0 M or (b) 1.0 M methanol in buffer without cryoprotectant (no sucrose). Instrument parameters and axis scaling as in Figure 2.

Figure 4 shows graphically the MLS and $g = 4.1$ amplitudes versus concentration for all alcohols. The relative amplitudes of $g = 4.1$ and MLS depend somewhat on the individual alcohol, as shown in Figure 4a and b. Determination of the slope of the line in modified Eadie−Hofstee plots (vide infra)[44] (not shown) gives an estimate of the apparent alcohol binding constants, $K_{d,glass}$,[45] for the $g = 4.1$ to MLS conversion. For the $g = 4.1$ suppression, $K_{d,glass}$ is quite similar for all four alcohols, ranging from 54 to 65 mM. The alcohol-binding constants for the MLS enhancement effect do not all fall in the same region, however, and extend from 23 mM (methanol) to 73 mM (ethanol), with the $K'_{d,glass}$ for 2-propanol (56 mM) and *n*-propanol (50 mM) falling in between. We note that these numbers are rather soft due to the paucity of data points used to generate them, but we emphasize that the full range of these alcohol concentrations that affect the S_2-state Mn EPR signals is well below the onset of the O_2 evolution inhibitory effects shown in Figure 1.

(44) Freifelder, D. *Physical Biochemistry*; W. H. Freeman: San Francisco, CA, 1982; pp 654−660.

(45) These dissociation constants must be distinguished from the conventional [physiological] K_d as they represent the binding properties in effect at the temperature that the EPR sample formed a solid glass and are labeled "glass" to indicate this defining condition.

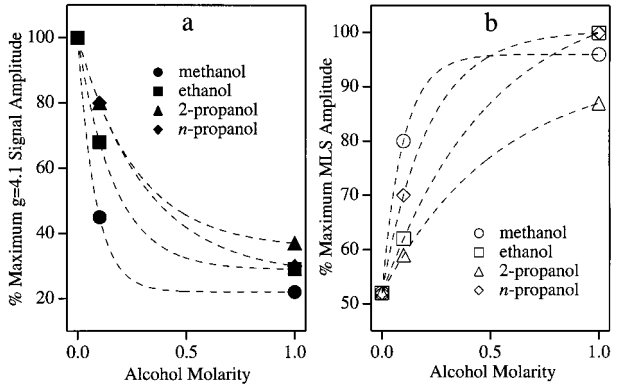

Figure 4. Effect of small alcohols on the relative amplitudes of PSII CW-EPR $g = 4.1$ (a) and MLS (b). Experimental data points are shown as markers. Samples originating from a single PSII preparation were divided into portions treated with either 1.0 M or 100 mM of the following alcohols: methanol, ethanol, 2-propanol, or *n*-propanol, as well as an alcohol-free (0 M) control. Background spectra obtained before illumination were subtracted. To account for any differences in sample concentration, spectra were then normalized to the amplitude of the $Y_D^{\bullet}$ signal before MLS and $g = 4.1$ peak-to-trough measurements were obtained; MLS intensity was determined by summing the features marked by asterisks in Figure 2. Instrument parameters for MLS and $g = 4.1$ spectra are as in Figure 2; those for Yd spectra (not shown) are microwave power, 80 μW; modulation amplitude, 1.6 G. The dashed lines are exponential fits to the data.

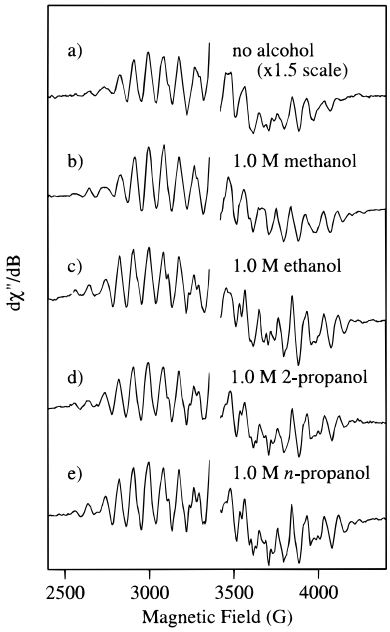

Figure 5. CW-EPR spectra showing the MLS region from PSII samples containing: (a) 0 M alcohol (control) and 1.0 M of the following: (b) methanol, (c) ethanol, (d) 2-propanol, and (e) *n*-propanol. Instrument parameters are as in Figure 2.

A careful examination of the hf peak patterns for all the 1.0 M alcohols (Figure 5) reveals that the effect of methanol on the MLS is distinct from the other three alcohols, which resemble one another closely as well as resemble the no-alcohol control. Most notably, the spectrum for the sample containing methanol shows less "dephasing" of the coincidence of the multiple ^{55}Mn hf lines around the third and fourth peaks upfield from $g = 2$. The 1.0, 2.0, and 5.0 M methanol-treated PSII CW-EPR spectra are also identical in peak position, number, and resolution (data not shown). The characteristic hf splitting pattern produced by any particular alcohol was consistent between PSII

preparations. Cycling the illuminated samples through either a 45 min or 4 h dark-adaptation on ice followed by reillumination also showed reproducible hf splitting patterns as well as CW-EPR signal intensity (up to three cycles were checked; data not shown).

The CW-EPR results clearly show that *all* of the alcohols used in these studies affect the magnetic properties of the Mn cluster. As such, they are interesting candidates for molecular probes of the ligation sphere of the Mn cluster. However, this CW-EPR evidence cannot demonstrate whether the spectroscopic effects observed result from direct ligation to Mn; for that we must turn to ESEEM.

ESEEM. ESEEM spectroscopy allows for selective detection of magnetic nuclei such as, ^{1}H, ^{2}H, ^{14}N, or ^{15}N proximal to the unpaired electron spins of the water-oxidizing Mn cluster.[30, 39, 46−48] The three-pulse ESEEM experiment is especially suited for detecting any deuterons from isotopically labeled alcohols which are weakly coupled to the Mn cluster, as the relatively slow (T_1 time scale) decay of the echo amplitude permits the observation of many modulation cycles,[49] yielding information about nuclei up to approximately 6 Å away from the metal center. Furthermore, the nature of the three-pulse technique allows one to suppress the contribution of proton modulation to the spectrum while simultaneously maximizing the contribution from exchanged ^{2}H (vide supra). The ESEEM contribution from deuterons on a labeled alcohol may be isolated from that of all of the other nuclei in the protein by ratioing the three-pulse time domain spectrum of the deuterated alcohol-treated membranes with the time domain of the natural-abundance alcohol sample.[36,46] This (^{2}H/^{1}H) ratio procedure acts to eliminate the contribution from the ^{14}N nuclei as well as most of any residual contribution from ^{1}H.

Such a ratioed time domain spectrum, acquired from parallel PSII samples containing 1.0 M methanol-d_4 and 1.0 M unlabeled methanol, is displayed in Figure 6a (top middle trace). In order to isolate the contribution of nuclei coupled to the OEC poised in the S_2-state, a background spectrum collected prior to illumination was subtracted from the illuminated time domain of each sample. These ^{2}H-labeled and natural-abundance methanol-treated PSII "illuminated minus dark" time domain data were each normalized to unity at the $T + \tau$ time corresponding to the maximum height of the first peak of the deuteron modulation pattern to account for any small differences in echo amplitude between the two parallel samples, then point by point ratioed, resulting in the time domain spectrum labeled "1.0 M methanol-d_4". The Fourier transform of the time domain ratio is shown in Figure 6b (middle trace). This spectrum exhibits a single peak centered around the ^{2}H Larmor frequency (2.1 MHz).

Figure 6 also includes the ratioed time and frequency domain spectra for parallel PSII samples prepared in 1.0 and 55 M (99.96% enrichment) $^{2}H_2O$ buffers. As evidenced by the insignificant height of the deuteron peak in the 1.0 M $^{2}H_2O$ spectrum compared to that of the 1.0 M methanol-d_4 spectrum, the relatively large ^{2}H peak obtained for the 1.0 M methanol sample is due to the methyl deuterons of the alcohol and *not*

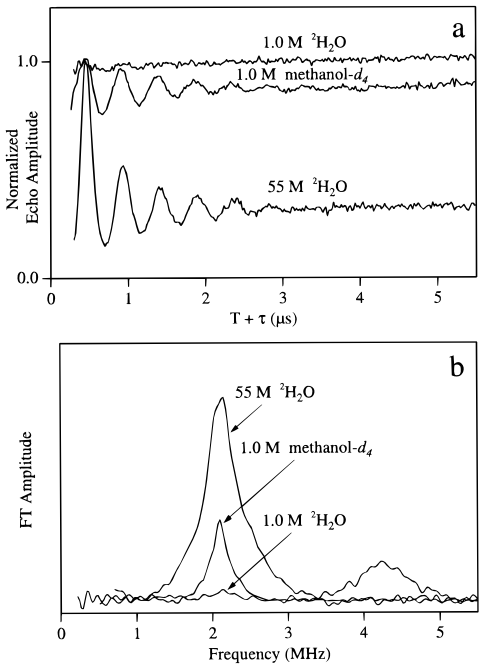

Figure 6. The three-pulse ESEEM (a) time domain ^{2}H/^{1}H ratios and (b) cosine Fourier transforms of the light-induced S_2 multiline signals obtained from PSII samples treated with 1.0 M methanol-d_4, 1.0 M $^{2}H_2O$, or 55 M $^{2}H_2O$. Background spectra obtained before illumination were subtracted prior to ratioing. Instrument parameters: microwave frequency, 9.26582 GHz; microwave power, 50 W; magnetic field, 3220 G; interpulse time τ, 219 ns; starting T, 81 ns; T increment, 20 ns; number of increments, 400; $\pi/2$ pulse, 15 ns; repetition rate, 200 Hz; temperature, 4.2 K.

from any $^{2}H_2O$, ^{2}HOH, etc., resulting from the rapid exchange of the alcoholic deuteron (which is only one-half of the ^{2}H concentration of the 1.0 M $^{2}H_2O$ sample) into the bulk solvent. Likewise, exchangeable deuterons from the alcoholic position of *any* of the alcohols at $\leq$1.0 M concentration make negligible contributions to the ESEEM deuteron peaks. Thus, the ESEEM spectra, dominated by the nonexchangeable ^{2}H nuclei of the deuterated alcohols, allow us to unambiguously determine whether or not the various alcohols bind in the immediate environment of the Mn cluster. The fully exchanged 55 M $^{2}H_2O$ spectrum (no alcohol) is included in Figure 6 for comparison. The shape of the large Fourier transform peak is indicative of both innersphere as well as outersphere contributions; deuterons strongly coupled to the Mn cluster give rise to the wide base of the ^{2}H peak in the frequency domain, and the combination peak at $2\nu_I$ reveals that there are multiple strongly coupled deuterons in the 55 M $^{2}H_2O$ sample.[50] We have interpreted these results as evidence of direct water or hydroxide ligation to Mn in the S_2-state.[30,41,50]

Figure 7, displaying the Fourier transforms of the ratioed ESEEM data in the 2.1 MHz Larmor frequency region, summarizes the results of the alcohol-treated PSII ESEEM studies. The data show clear distinctions in the accessibility of the different alcohols to binding sites proximal to the Mn cluster. In comparing all of the 1.0 M data, the smaller alcohols methanol and ethanol show the largest ^{2}H peak intensities, the longer *n*-propanol shows less intensity, and the relatively rotund 2-propanol shows none above the level of its exchangeable alcoholic ^{2}H. A minuscule ^{2}H peak is also observed for DMSO. These trends indicate that the smaller alcohols methanol, ethanol,

(46) Force, D. A.; Randall, D. W.; Britt, R. D. *Biochemistry* **1997**, *36*, 12062−12070.
(47) Tang, X.-S.; Diner, B. A.; Larsen, B. S.; Gilchrist, M. L.; Lorigan, G. A.; Britt, R. D. *Proc. Natl. Acad. Sci. U.S.A.* **1994**, *91*, 704−708.
(48) Britt, R. D. In *Biophysical Techniques in Photosynthesis*; Amesz, J., Hoff, A. J., Eds.; Kluwer Academic: Dordrecht, The Netherlands, 1996; pp 235−253.
(49) Mims, W. B.; Peisach, J. *Electron Spin−Echo Spectroscopy and the Study of Metalloproteins*, Plenum Press: New York, 1981; pp 213−263.
(50) Gilchrist, M. L. Ph.D. Dissertation. Department of Chemistry, University of California, Davis, 1996.

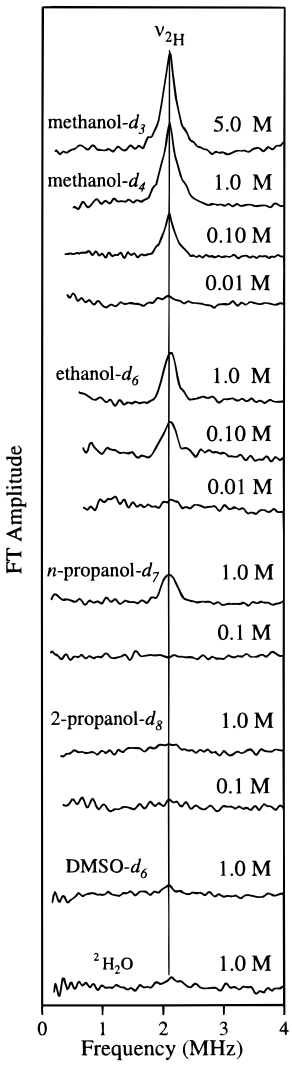

Figure 7. The cosine Fourier transforms of the three-pulse ESEEM time domain ($^2H/^1H$) ratios of the light-induced S_2 multiline signals obtained from alcohol-treated PSII samples. The traces are grouped by the specific deuterated alcohol used, with the alcohol concentrations as indicated, and are offset for clarity. A single isotopic labeling was used for each alcohol with the exception of methanol. Deuterated methanol samples were treated with $C^2H_3O^1H$ (5.0 M) or $C^2H_3O^2H$ (all other molarities). Fourier transforms of the 1.0 M ^2H_2O and 1.0 M DMSO-d_6 treated samples are included for comparison. Instrument parameters are as in Figure 6.

and *n*-propanol bind near the Mn cluster, while the bulkier 2-propanol and DMSO do not ($r_{eff} \geq 6$ Å).

The ESEEM peak heights are also utilized to determine effective binding constants for methanol and ethanol, as shown in the modified Eadie−Hofstee graph in Figure 8. The area under the ESEEM FT peak,[51] which reflects the concentration of alcohol bound in the sites proximal to Mn, is plotted versus the area divided by the alcohol concentration in the solvent buffer. By its linearity, the graph indicates a single binding site (or multiple sites with very similar binding constants); using linear regression the negative slope of the line yields a nonphysiological $K_{d,glass} = 79$ mM ($\sigma = 16$) for methanol and $K_{d,glass} = 82$ mM ($\sigma = 21$) for ethanol.[45] The *y*-intercepts correspond to binding site saturation;[52] although we cannot

(51) The ESEEM FT line widths are independent of alcohol concentration, suggesting a single mode of alcohol binding. Also, the estimated $K_{d,glass}$ values are on the order of 1000 times greater than the ~100 μM maximal PSII concentration.

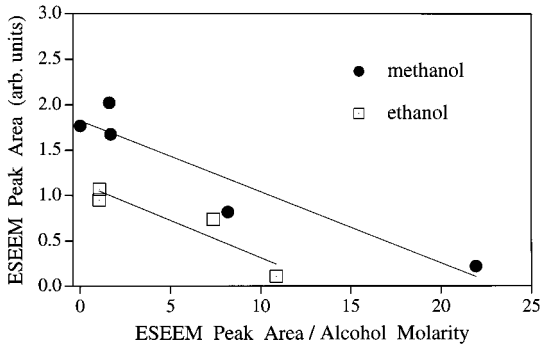

Figure 8. Modified Eadie−Hofstee plot of the dependence of the three-pulse ESEEM Fourier transform peak area on alcohol concentration for methanol- (circles) and ethanol- (squares) treated PSII samples. The lines are a linear regression fit to the data. The slope of the line yields a $K_{d,glass}$ of 79 mM ($\sigma = 16$) for methanol and 82 mM ($\sigma = 21$) for ethanol.

extract the absolute number of binding sites from the data, the plot may be used to illustrate that the samples with the higher concentration of alcohol are under saturating conditions with regards to the OEC alcohol binding site(s): the data points for those samples approximate the *y*-intercept value.

There are reports in the literature that although S-state turnover (i.e., electron transfer) is known to occur at 200 K, associated ligand exchange may not take place until after the sample is warmed to a higher temperature in an "annealing" step.[39,53] Consequently, we have used dark-annealing of PSII samples for 1 min at ice temperature following 200 K illumination to test for alcohol exchange following the S_1 to S_2 oxidation.[39] This annealing approach was taken with four sets of $^2H/^1H$ alcohol-treated PSII samples: 1.0 M or 100 mM ethanol and methanol in the presence of PPBQ. No significant spectral changes were induced by the annealing step; the results of one typical study, the 1.0 M ethanol treatment, are displayed in Figure 9. The time domain patterns and resulting Fourier transforms are essentially the same for the light-minus-dark and the annealed-minus-dark spectra. However, we note that this is not conclusive evidence that ligand exchange did *not* occur; others have presented evidence for ligand exchange at or below 200 K.[54]

Discussion

A. O_2 Evolution. Concentrations of methanol[28] and ethanol[55] $\leq$ 1.0 M have been previously reported to leave the oxygen evolution rate unchanged from that of untreated PSII preparations; our results are in general agreement with these findings. Our investigations have further characterized these effects by extending the alcohol concentrations used in the oxygen evolution assay up to 5.0 M as well as examining the effects of the larger alcohols 2-propanol and *n*-propanol. We have established a threshold of OEC impairment for each alcohol and shown that inhibition of oxygen evolution requires much higher alcohol concentrations than the concentrations that affect the proportion of multiline versus $g = 4.1$ signal forms or that are required for ESEEM detected binding. The mode of this

(52) Fersht, A. *Enzyme Structure and Mechanism*; W. H. Freeman: New York, 1985; p 191.
(53) Beck, W. F.; dePaula, J. C.; Brudvig, G. W. *J. Am. Chem. Soc.* **1986**, *108*, 4018−4022.
(54) Boussac, A.; Rutherford, A. W.; Styring, S. *Biochemistry* **1990**, *29*, 24−32.
(55) Andrèasson, L.-E. In *Current Research in Photosynthesis*; Baltscheffsky, M., Ed.; Kluwer Academic: Dordrecht, The Netherlands, 1990; pp 785−788.

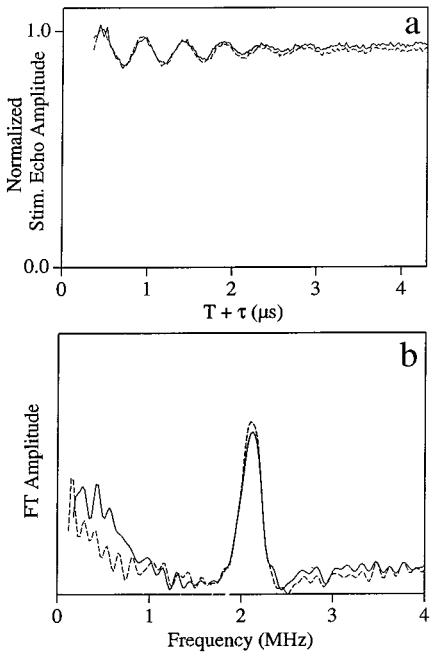

Figure 9. The three-pulse ESEEM (a) time domain $^2H/^1H$ ratios and (b) cosine Fourier transforms of the light-induced (dashed traces) and annealed (solid traces) S_2 multiline signals obtained from PSII samples treated with 1.0 M ethanol. The annealing treatment consisted of warming the illuminated sample to 4 °C for 1 min in the dark before freezing to 77 K. Instrument parameters are as in Figure 6.

inhibitory action, observed to be fully reversible for the modest impairment induced by 5.0 M methanol, but less reversible for the more damaging *n*-propanol and 2-propanol, remains to be determined; possibilities include changes in the binding of the extrinsic proteins or the integrity of the membranes themselves.[56]

B. CW-EPR. All of the alcohols examined act to convert the $g = 4.1$ signal to the MLS. This implies that the induction of the $g = 4.1$ to MLS spin state conversion is a generic property of small alcohols. The magnitude of conversion for each alcohol is slightly different, particularly in production of the MLS, and this could indicate that the different alcohols induce similar, but not identical, changes in the pattern of exchange couplings within the cluster, all of which are sufficient to alter the ground spin state of the Mn complex at the higher alcohol concentrations. However, it is clear from comparing the ESEEM and spin state conversion results that the EPR signal interconversion cannot be induced solely by the direct binding of the alcohols to the Mn cluster. 2-Propanol provides the clearest counterexample: it triggers the signal interconversion (Figure 4) but does not appear to bind directly to the Mn cluster (Figure 7). We cannot rule out the possibility that direct binding of the smaller alcohols contribute to the spin state conversion, but would argue against this being the sole source of the conversion since the $K_{d,glass}$ values for binding are generally higher than the estimated $K_{d,glass}$ values for the increased multiline formation, by a factor in excess of 3 for methanol, the alcohol with the greatest discrepancy. We also note that methanol, the most effective at producing the MLS form at a given molarity, also appears to produce subtle differences in the MLS line shape (Figure 5). The fact that the estimated $K_{d,glass}$ values for MLS enhancement do not perfectly match those for diminution of the $g = 4.1$ signal suggests that other spin states, not as readily EPR observable, may also be populated at the 7 K observation temperature.[57−59]

C. ESEEM. It is important to determine whether these various alcohols ligate directly to the Mn cluster of the OEC and, if so, to determine possible binding geometries. Since the dipolar hyperfine interactions measured via ESEEM are sensitive to the distances between the Mn ions of the cluster and the alcohol-introduced deuterons, analysis of the ESEEM results can provide direct evidence concerning the alcohol binding motifs.

Point Dipole ESEEM Analyses. We begin with the simplest method of analysis, employing a "single nucleus/equivalent nuclei" approximation,[60] in conjunction with an analytical modulation depth characterization and a simple point dipole approximation for the Mn cluster, to get a coarse measure of the distances of deuterons coupled to the Mn cluster. This approach provides immediate insights into whether a deuterated ligand is bound to a metal center and serves as a starting point for more elaborate numerical simulations. For each alcohol, an average ^2H modulation depth parameter ($\bar{k}$) is measured from the three-pulse time domain pattern, and the radial distance r from the assumed electron point dipole to the deuteron(s) is calculated based on the $\bar{k} \propto r^{-6}$ distance dependence.[61−63] In the single nucleus approximation, which gives a good measure of a lower distance limit, the entire amplitude of the modulation is assumed to arise from the closest single deuterium nucleus, which is assumed to dominate because of the dramatic dropoff with distance of the r^{-6} function. The equivalent nuclei approximation, providing an upper distance limit, assumes that the signal amplitude has an equal contribution from *all* chemically relevant deuterons. For methanol, using the ratioed three-pulse modulation shown in Figure 10, this provides a distance range between 2.9 and 3.7 Å (Table 1). The distance

(56) For example, anesthetics [including some small alcohols] have been implicated in the conformational alteration of erythrocyte membranes/proteins. See: Seeman, P.; Roth, S.; Schneider, H. *Biochim. Biophys. Acta* **1971**, *225*, 171−184. Seeman, P.; Chau, M.; Goldberg, M.; Sauks, T.; Sax, L. *Biochim. Biophys. Acta* **1971**, *225*, 185−193. Schneider, H. *Biochim. Biophys. Acta* **1968**, *163*, 451−458.

(57) The alcohol effects are not directly correlated with generic cryoprotection. Different cryoprotectants differentially affect the ratio of $g = 4.1$ to MLS, and in comparing Figures 2 and 3 one observes that the $g = 4.1$ to MLS ratio is actually smaller with no cryoprotectant at all, whereas the addition of methanol, with or without sucrose, favors the MLS.

(58) Smith, P. J.; Pace, R. J. *Biochim. Biophys. Acta* **1996**, *1275*, 213−220.

(59) Boussac, A.; Un, S.; Horner, O.; Rutherford, A. W. *Biochemistry* **1998**, *37*, 4001−4007.

(60) Halkides, C. J.; Farrar, C. T.; Larsen, R. G.; Redfield, A. G.; Singel, D. J. *Biochemistry* **1994**, *33*, 4019−4035.

(61) Lorigan, G. A.; Britt, R. D.; Kim, J. H.; Hille, R. *Biochim. Biophys. Acta* **1994**, *1185*, 284−294.

(62) Mims, W. B.; Davis, J. L.; Peisach, J. *J. Magn. Res.* **1990**, *86*, 273−292.

(63) The modulation depth parameter (k) is related to the distance between a weakly coupled ^2H nucleus and paramagnetic center by:[61,62] $k = 6(g\beta/H_o r^3)^2 \sin^2(2\theta)$ where g is the electronic g factor, β is the Bohr magneton for an electron, H_o is the magnitude of the applied magnetic field, θ is the angle between the magnetic field vector and the vector connecting the electron and ^2H, and r is the distance between the electron and ^2H. We are neglecting the effect of the electric quadrupole in this expression. In order to account for all of the possible orientations of the electron-nucleus position vector with respect to the magnetic field, the previous equation is averaged over the unit sphere, resulting in the following expression: $\bar{k} = {}^{16}/_{5}(g\beta/H_o r^3)^2$ where $\bar{k}$ represents this spherical average of the modulation depth parameter. Furthermore, we need to account for the modulation decay, which occurs at a rate dependent upon the magnitude of the hyperfine anisotropy induced by the dipolar interaction ($\propto r^{-3}$) between the paramagnetic center and the nucleus. The decay factor for a single $I = 1$ ^2H nucleus with dipolar coupling is given by $\cos[0.378(m\pi/r^3)(g\beta/H_o)]$ where the integer m depends on the $(T + \tau)$ time corresponding to the center of the particular modulation cycle from which the experimental modulation depth measurement was taken, and is equal to 3 for the calculations made herein. Multiplying the average modulation depth parameter ($\bar{k}$) by the decay factor results in a corrected modulation depth expression which can be compared to the calculated modulation depth taken from the experimental data and used to obtain distance estimates in the "single nucleus/multiple equivalent nuclei" approximations.

Table 1. Point Dipole Radial Distance between Alcohol Deuterons and OEC Mn determined by Simulating the Modulation Depth Parameter ($\bar{k}$) and the Three-Pulse ESEEM Time Domain Patterns

alcohol[a]	simulation method	(no. of nuclei)	point dipole radial distance (Å)		
methanol	single nucleus[b]	(1)	2.9		
	equivalent nuclei[b]	(3)	3.7	3.7	3.7
	inequivalent nuclei[c]	(3)	3.0	3.9	4.1
ethanol	single nucleus[b]	(1)	3.3		
	equivalent nuclei[b]	(2)	3.8	3.8	
		(3)	4.1	4.1	4.1
	inequivalent nuclei[c]	(2)	3.5	4.1	

[a] Alcohols added to PSII preparations; see text for details. [b] Approximation used in conjunction with modulation depth parameter ($\bar{k}$) calculations. [c] Determined from best-fit simulation to the experimental data, as shown in Figure 10.

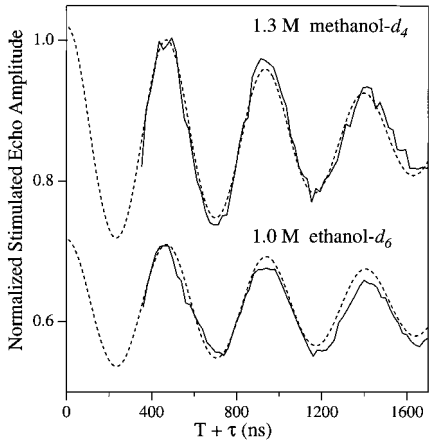

Figure 10. Three-pulse ESEEM time domain $^2H/^1H$ ratios of the light-induced S_2 signal obtained from PSII preparations containing 1.3 M methanol-d_4 (upper trace) and 1.0 M ethanol-d_6 (lower trace). Background spectra obtained before illumination were subtracted prior to normalizing the time domains to account for any differences in echo amplitude. The time domain traces have the same *y*-axis scale but are offset for clarity. Each dotted line displays the best-fit result from numerical simulations of the ESEEM spectra, with the modulation arising from (upper trace) three dipolar coupled deuterons with proton-scaled couplings of 2.92, 1.33, and 1.15 MHz (3.0, 3.9, and 4.1 Å distances using a point dipole model) and (lower trace) two dipolar coupled deuterons with proton-scaled couplings of 1.82 and 1.15 MHz (3.5 and 4.1 Å distances using a point dipole model). Instrument parameters as in Figure 6. Simulation parameters were the following: $A_{iso} = 0.0$ MHz; $\nu^2_H = 2.105$ MHz; nuclear quadrupole coupling constant (e^2Qq) = 0.22 MHz; electric field gradient asymmetry parameter (η) = 0.1; $\tau = 219$ ns.

range from this simple analysis is rather narrow because a factor of 3 in spin numbers is highly compressed in the corresponding distances by the steep r^{-6} dependence.[60] The basic result of this simple calculation is clear: methanol binds close enough to Mn that it could be a direct ligand. The modulation depth for ethanol is smaller than for methanol (Figure 10), resulting in a minimum 3.3 Å single nucleus distance, and maximal 3.8 or 4.0 Å distances for two equivalent methylene or three equivalent methyl deuterons (Table 1). Again, these distances are consistent with direct ethanol binding.

Improved distance estimates are obtained by simulating the experimental ESEEM data using a numerical algorithm[39] based upon the density matrix formalism.[38] Figure 10 also shows the best-fit simulations (dashed lines) as overlays to the experimental data for methanol- and ethanol-treated PSII; the simulations include the effect of the deuteron quadrupole interaction (e^2Qq = 0.22 MHz, $\eta = 0.1$), but assume zero isotropic hyperfine interaction[40] and are optimized to match both the initial modulation depth and the decay over three cycles of the three-pulse time domain patterns. The simulation overlaying the experimental ratioed ESEEM spectrum for the 1.3 M methanol-d_4/unlabeled methanol PSII samples in Figure 10 results from three inequivalent methanol deuterons with dipolar interactions (T_{dip}) of 1.15 (0.176), 1.33 (0.205), and 2.92 (0.449) MHz, where the parenthetical value is for the deuteron, and the lead value is scaled to the corresponding proton coupling using the ratio of the respective moments. (We choose to emphasize the scaled proton values for comparison to our ENDOR (electron nuclear double resonance) study of water ligation.[30]) These couplings correspond to point dipole distances of 3.0, 3.9, and 4.1 Å (Table 1). Poorer simulations result from utilizing more than three coupled deuterons (not shown), because to maintain the proper initial modulation depth, these deuterons must be more weakly coupled (more distant), and this results in less damping of the modulation over successive cycles than is experimentally observed. Since the simulated ESEEM data were obtained at a saturating level of methanol (Figure 8), these data and simulations indicate that a single methanol ligand binds to the Mn cluster. We note that these simulations do not require the addition of distant "matrix" deuterons as was the case for our previous model complex work.[40] Our interpretation is that the small dinuclear Mn cluster is completed surrounded by solvent containing the deuterated methanol, whereas the PSII Mn cluster is surrounded by protein in all directions except along a narrow binding cleft (vide infra).

A good fit is obtained for the 1.0 M ethanol-d_6 treatment case using two inequivalent deuterons with $T_{dip} = 1.84$ (0.283) and 1.14 (0.175) MHz, corresponding to 3.5 and 4.1 Å radial distances (Table 1). We consider the smaller modulation of the ethanol sample and the adequacy of the 2-deuteron fit to be consistent with the alcohols binding via direct Mn ligation to the alcohol oxygens, resulting in similar ranges of distances for the methyl deuterons of methanol and the methylene deuterons of ethanol, but with smaller modulation from ethanol due to having one less deuteron at this close range. Such a ligation geometry places the three methyl deuterons of ethanol to greater distance, where the steep r^{-6} minimizes their contribution relative to the closer methylene deuterons. Any small contribution they make will lead to a slight overestimation to the methylene couplings in the two-deuteron simulation, so the distances should be considered minimal, but approximately correct within the constraints of the point dipole approximation. As for the methanol case, the ethanol simulation indicates ligation by a single ethanol ligand.

Comparison with Model Studies. Randall et al.[40] described ENDOR and ESEEM studies of both water and methanol ligation to the Mn(III) ion of a dinuclear μ-alkoxo-bridged Mn(III)Mn(IV) complex. These experiments show that the alcoholic proton of methanol has an identical dipolar interaction to that of one water proton, and thus both protons are similarly positioned with respect to the Mn cluster. The three-pulse ESEEM patterns for the methyl-deuterated methanol adduct were best simulated with Mn(III)−H distances of 3.0, 3.5, and 4.0 Å. The 3.0, 3.9, and 4.1 Å radial distances we have obtained in our methanol PSII simulations compare very well with these values; thus, in addition to providing clear evidence for small alcohols binding in proximity to the catalytic center of PSII, our data is consistent with that binding occurring directly via a Mn−alcohol oxygen bond. In addition, the K_d value for methanol ligation for this Mn(III)Mn(IV) complex is 80 mM,[64] virtually identical to that obtained for our OEC Mn methanol binding site.

Scheme 1. Geometric Models of the Tetranuclear Mn Cluster of the OEC

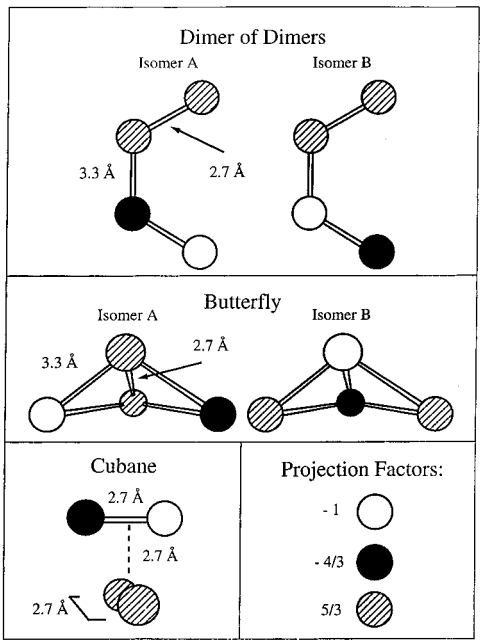

Coupled Cluster Simulations. As discussed by Randall et al.[40,65] and others,[66−69] analysis of proton/deuteron dipolar hyperfine interactions for dinuclear metal clusters (and by extension, tetranuclear metal clusters) is considerably more complex than for a single metal ion case, where a simple point dipole approximation may be adequate. The hydrogen nuclei of the ligands experience dipolar interactions with each of the metal ions. To a first degree of approximation beyond the simple single point dipole approximation, each metal center can be treated as a separate point dipole with an effective "projection factor" resulting from coupling the isolated ions into an effective spin for the cluster, and which therefore depends on the total spin of each individual ion, which is determined by its oxidation state. On the basis of the work of DeRose et al.[66] for a dinuclear non-heme iron system, Fiege et al.,[68] Randall et al.,[40] and Willems et al.[69] have developed analytical expressions for the matrix components of the resulting hyperfine interaction tensor for a dinuclear metal cluster. We generalize this approach for tetranuclear clusters of specific geometries and spin projection factors using a numerical approach described in detail in the Appendix.

Several core OEC configurations from the literature are represented in Scheme 1. Specifically, the Berkeley "dimer-of-dimers" model,[70] a "butterfly" model,[71] and a symmetric "cubane" model are shown,[72] along with relevant bond distances. For this work we focus on the dimer-of-dimers and cubane models as examples of a relatively extended, asymmetric configuration and a more confined, symmetric one. We utilize the spin projection factors of Zheng and Dismukes[73] that provide a reasonable basis of analysis of both MLS EPR and ^{55}Mn ENDOR spectra.[74]

Berkeley "Dimer-of-Dimers" Model: Isosurfaces and Contours. We have calculated the hyperfine tensors for the OEC by using the numerical methods described in the Appendix. The middle-valued component of the hyperfine interaction tensor, A_{mid}, gives the most intense feature in an ENDOR powder pattern, and we consider it to have the most significant influence on the deuteron ESEEM patterns. Figures 11a−d illustrate three-dimensional constant-valued isosurfaces of A_{mid} using the Berkeley model for the Mn cluster.[70] Figures 11a′−c′ show corresponding two-dimensional sectional slices through the three-dimensional isosurfaces. The isosurfaces can be thought of as shells around the Mn cluster where the interpolated A_{mid} is consistent with the values observed for non-exchangeable methanol protons in the immediate environment of the Mn cluster (±2.92, ±1.33, and ±1.15 MHz). The outer two isosurfaces are rendered translucent in order to reveal the innermost [2.92 MHz] isosurface. If this arrangement were correct for the Mn ions in the OEC, a proton located anywhere on each of these shells would be consistent with the experimentally measured dipolar hyperfine interaction. We assume in constructing the geometric model that the four Mn ions in this model are coplanar. Since the experimental methods employed to determine the dipolar hyperfine interaction are insensitive to the sign of the dipolar hyperfine interaction, isosurfaces where A_{mid} is either negative (dark and corresponding translucent isosurfaces) or positive (light isosurfaces) are shown. With the spin projection factors of Zheng and Dismukes,[73] two "magnetic isomers" are possible for the dimer-of-dimers geometrical arrangement, as depicted in Scheme 1. In isomer A, the Mn with projection factor −1 is in a terminal position, and in isomer B it occupies a central position. Figure 11 shows the isosurfaces for this latter magnetic isomer. We note here that the A isomer isosurfaces are qualitatively similar in appearance (not shown), as isosurface radial distances are not greatly affected by the small changes of the spin projection factor. The hyperfine tensor rhombicities, χ, are displayed by the dotted, nonconcentric lines in the sectional slices. These vary substantially across a given A_{mid} isosurface. Though ESEEM is less sensitive than ENDOR to line shape dependent parameters such as rhombicity, it is likely that simulations of the ESEEM patterns would not match the spectral data as well as they do if the rhombicity of the hyperfine interaction were to approach unity.[75]

The longest Mn−H distances in these slices are found at the terminal Mn of the ($^5/_3$, $^5/_3$) spin projection factor dimer: 3.7 Å for the strongest interaction (2.92 MHz) and 5.6 Å for the weakest (1.15 MHz). These distances are summarized in Table 2, along with analogous maximum distance values for the other dimer-of-dimers magnetic isomer, as well as the butterfly and cubane models.

Cubane Model: Isosurfaces and Contours. The symmetric cubane model is more compact than the dimer-of-dimers model and does not present multiple magnetic isomers. Figure 12 shows three-dimensional isosurfaces and two-dimensional slices for three different orientations of the cubane geometry. As noted

(64) Pecoraro, V. L. Personal communication.
(65) Randall, D. W.; Chan, M. K.; Armstrong, W. H.; Britt, R. D. *Mol. Phys.* **1998**, *95*, 1283−1294.
(66) DeRose, V. J.; Liu, K. E.; Lippard, S. J.; Hoffman, B. M. *J. Am. Chem. Soc.* **1996**, *118*, 121−134.
(67) Khangulov, S.; Sivaraja, M.; Barynin, V. V.; Dismukes, G. C. *Biochemistry* **1993**, *32*, 4912−4924.
(68) Fiege, R.; Zweygart, W.; Bittl, R.; Adir, N.; Genger, G.; Lubitz, W. *Photosyn. Res.* **1996**, *48*, 227−237.
(69) Willems, J. P.; Lee, H. I.; Burdi, D.; Doan, P. E.; Stubbe, J.; Hoffman, B. M. *J. Am. Chem. Soc.* **1997**, *119*, 9816−9824.
(70) Yachandra, V. K.; DeRose, V. J.; Latimer, M. J.; Mukerji, I.; Sauer, K.; Klein, M. P. *Science* **1993**, *260*, 675−679.
(71) Christou, G.; Vincent, J. B. *Biochim. Biophys. Acta* **1987**, *895*, 259−274.
(72) Brudvig, G. W.; Crabtree, R. H. *Proc. Natl. Acad. Sci. U.S.A.* **1986**, *83*, 4586−4588.
(73) Zheng, M.; Dismukes, G. C. *Inorg. Chem.* **1996**, *35*, 3307−3319.
(74) Randall, D. W.; Sturgeon, B. E.; Ball, J. A.; Lorigan, G. A.; Chan, M. K.; Klein, M. P.; Armstrong, W. H.; Britt, R. D. *J. Am. Chem. Soc.* **1995**, *117*, 11780−11789.
(75) Reijerse, E. J.; Keijzers, C. P. *J. Magn. Res.* **1987**, *71*, 83−96.

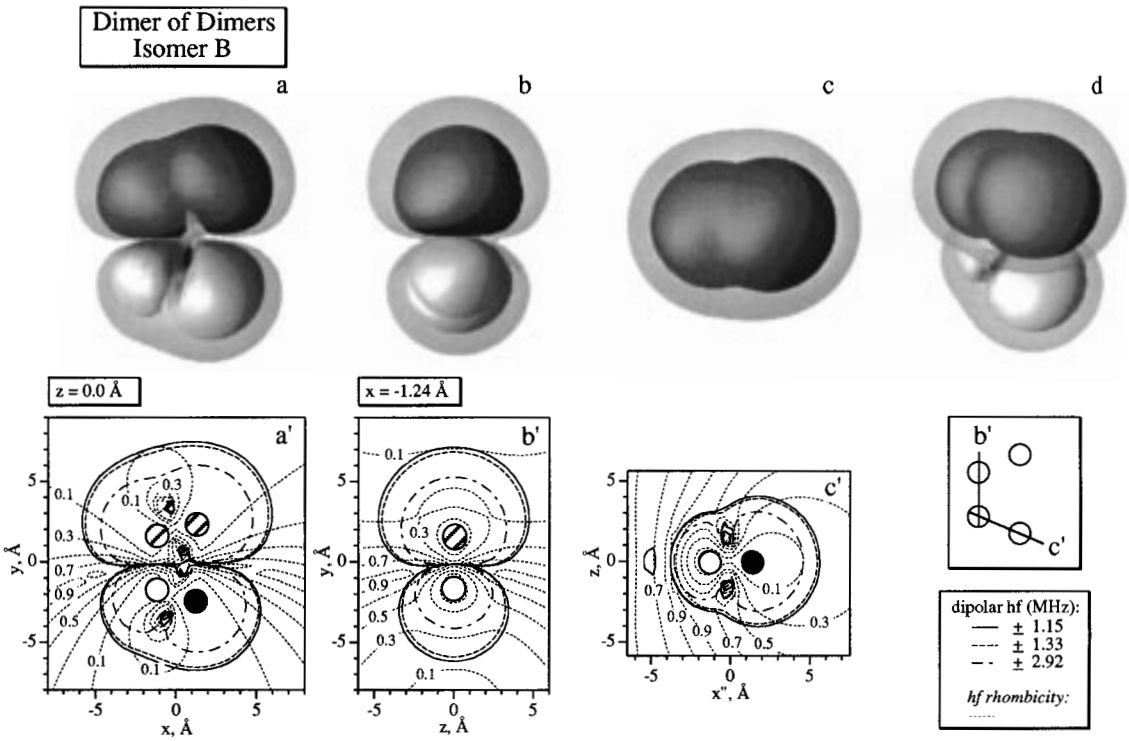

Figure 11. Hyperfine isosurfaces (a−d) and isosurface slices (a′−c′) for the Berkeley dimer-of-dimers model of the tetranuclear Mn cluster of PSII. The first three isosurface figures present a viewpoint from each of the Cartesian planes (a) *xy*, (b) *zy*, and (c) *xz*; the last shows an off-axis view (d). The outer isosurface is translucent to reveal the innermost ±2.92 MHz isosurface. Negative hyperfine values are shown as dark isosurfaces, positive values are as light isosurfaces. The contour plots below each isosurface show the corresponding planar slices through the Mn ions, taken as orthogonal slices at the boxed values or as indicated in the upper legend. The dipolar hyperfine traces are shown as solid lines for ±1.15 MHz, short dashes for ±1.33 MHz, and dash−dot lines for ±2.92 MHz. The hf rhombicity is indicated by dotted lines; the values are labeled on each line. Projection factors are the same as those shown in Scheme 1.

Table 2. Maximum Radial Mn−H Distances Obtained from the Strongest and Weakest Dipolar hf Interaction[a] (T_{dip}) for Methanol

		r_{max} (Å) associated with	
model[b]	isomer	$T_{dip} = \pm 2.92$ MHz	$T_{dip} = \pm 1.15$ MHz
dimer-of-dimers	A	3.7	5.5
dimer-of-dimers	B	3.7	5.6
butterfly	A	3.5	4.7
butterfly	B	3.4	4.5
cubane		3.6	4.9

[a] Using the contours of constant dipolar hf coupling, as shown in Figures 11 and 12. [b] Simple geometric model for the Mn cluster of the OEC as shown in Scheme 1.

in Table 2, maximal Mn−H distances for the compact cubane geometry are shorter than for the more extended dimer-of-dimers geometry.

Berkeley "Dimer-of-Dimers" Model: Alcohol Binding Motifs. Given the isosurfaces constructed above, we can construct molecular models for alcohol binding to the various cluster geometry models. For example, Figure 13 displays axial and equatorial binding configurations for methanol bound to the ($-^4/_3$ projection factor) Mn of the dimer-of-dimers B isomer. We see that direct Mn coordination by methanol through the alcoholic oxygen is perfectly consistent with magnetic parameters analyzed via this tetrapoint dipole-modeling treatment. Clearly the actual detailed binding geometry is extremely underdetermined: we do not even know with certainty the correct core structure for the Mn cluster. However, the fact that all models tested give reasonable Mn−H distance ranges for direct alcohol coordination provide strong evidence that methanol and ethanol indeed ligate to the Mn cluster in the S_2-state. Moreover, the ESEEM simulations strongly suggest that only one methanol or ethanol molecule binds.

D. Binding Site Accessibility. The preceding data and analysis provides evidence that one methanol or ethanol molecule can bind to the Mn cluster in the S_2-state, with a binding constant on the order of 80 mM. From our analysis of the ethanol data, attributing the major modulation as arising from the two methylene deuterons of the carbon adjacent to the alcohol OH group, one would expect comparable intensity from *n*-propanol if it bound to the Mn cluster with the same affinity and accessibility. However, we note that only at the highest (1.0 M) concentration do we observe appreciable ^{2}H modulation from *n*-propanol, and even then the peak has only 55% of the amplitude of the equivalent ethanol peak. There is no detectable peak associated with the 0.1 M concentration data, even though that concentration is large enough to provide a large fractional population if *n*-propanol also bound to Mn with the same 80 mM binding constants of methanol and ethanol. We therefore conclude that, though not fully prohibited, access of *n*-propanol is limited relative to the smaller methanol and ethanol molecules. The trend continues to the bulkier 2-propanol, and the sole nonalcohol probe, DMSO, both of which exhibit minuscule peak heights even at 1 M concentration. The most straightforward interpretation of these trends is that the larger bulkier probes cannot readily access the Mn cluster because of an access channel of limited size. Such controlled access to the Mn cluster has been postulated before[76] on water oxidation mechanistic grounds. Thus, the *n*-propanol access could be limited due to greater steric hindrance (such as an angled pocket shape or an amino acid acting as a stile) than confronted by the shorter ethanol molecule, while 2-propanol and DMSO could have completely blocked access due to their large diameters. In this

(76) Wydrzynski, T.; Hillier, W.; Messinger, J. *Physiol. Plantarum* **1996**, *96*, 342−350.

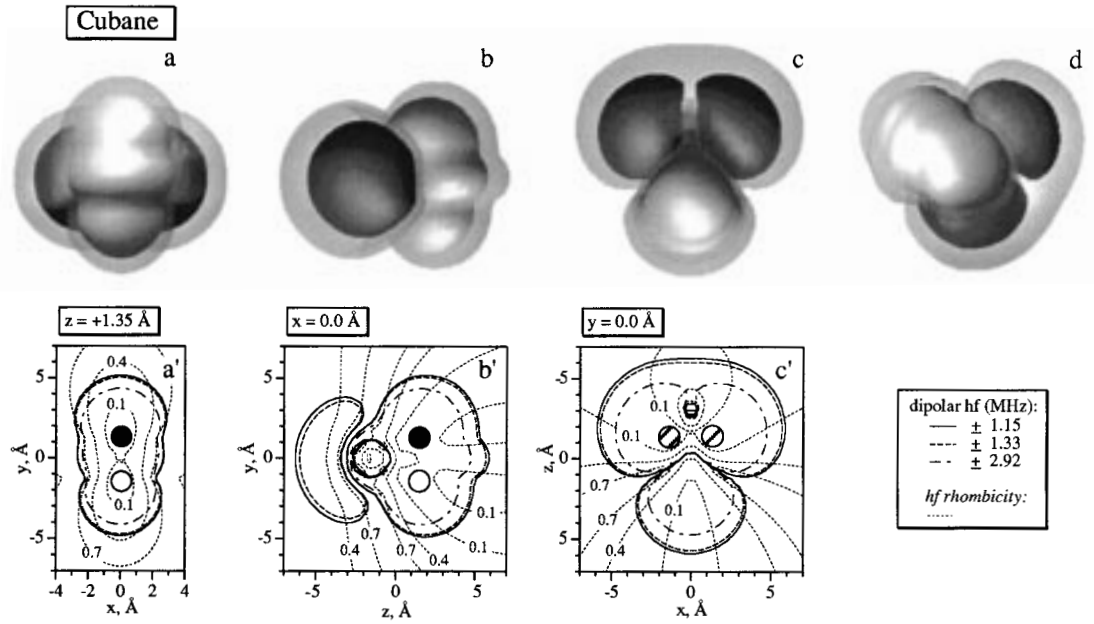

Figure 12. Hyperfine isosurfaces (a−d) and isosurface slices (a′−c′) for the Cubane model of the tetranuclear Mn cluster of PSII. The isosurface viewpoints and configuration are the same as in Figure 11. The contour plots below each isosurface show the corresponding planar slices through two of the Mn ions, taken as follows: (a′) *xy* slice at $z = +1.35$ Å; (b′) *zy* slice at $x = 0.0$ Å; (c′) *xz* slice at $y = 0.0$ Å. The dipolar hyperfine traces are the same as in Figure 11. The hf rhombicity is indicated by dotted lines; the values are labeled on each line. Projection factors are the same as those shown in Scheme 1.

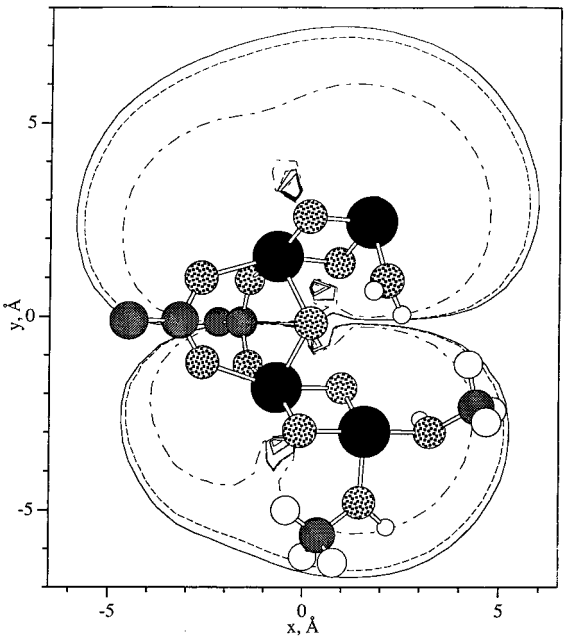

Figure 13. Molecular model of the tetranuclear Mn cluster of PSII superimposed on the hyperfine isosurface slice from Figure 11a′. Two representative binding motifs (equatorial and axial) to a terminal Mn (projection factor $-4/3$) are displayed. A water is shown bound to the other terminal Mn (projection factor $5/3$). Although we show two possible binding motifs, the experimental ESEEM amplitude and simulation indicate that only one methanol is bound to the cluster. We cannot rule out other binding geometries, such as a deprotonated alcoxide providing a bridge between Mn ions. Atom key: Mn (black); O (speckled); C (stripe); H (white). Mn and methanol bond lengths: Mn−O(methanol), 2.1 Å; O−H, 1.0 Å; O−C, 1.4 Å; C−H, 1.1 Å. Radial Mn−H(methanol CH_3) distances: (axial) 3.1, 3.8, and 3.9 Å; (equatorial) 3.4, 3.4, and 3.9 Å.

case, using conventional bond lengths and van der Waals radii as a guide, we can estimate the effective Mn cluster "access-channel" diameter to be in the 3−4 Å range.[77] Alternate explanations of the binding trends would invoke physical/chemical properties other than size. If binding site hydrophilicity were the controlling feature, consistent with tight binding of the most hydrophilic probes methanol and ethanol, one would expect 2-propanol to bind as well or better than *n*-propanol,[78] which it does not. The relative Lewis basicity of these four alcohols and DMSO for binding to the hard Mn(III) and Mn(IV) Lewis acids would also affect the strength of binding. However, one would expect the basicities of ethanol and *n*-propanol to be essentially identical, yet ethanol is observed to bind preferentially. Thus, on the basis of the proximity trends evidenced by the ESEEM data (Figure 7), we postulate that accessibility is indeed playing a major role in determining the relative binding of the different alcohols.

E. Alcohol versus Water Ligation. Our evidence for small alcohol binding at the S_2-state complements our ^{2}H ESEEM and ^{1}H ENDOR studies of water binding at this state.[30, 50] In that work, we identify a class of exchangeable hydrogens with a strong (4.9 MHz) ^{1}H dipolar coupling, consistent with Mn-bound water or hydroxide, and in conflict with some other recent ESEEM[79] and ENDOR[80] studies that argue against water

(77) This range is based on a model where the alcohol functionality is set along the *z*-axis so the *xy*-plane is the minimal plane of approach facilitating Mn−O binding, and the channel diameter is the cylindrical cross-section which circumscribes the molecular *xy*-projection. The model uses methanol and 2-propanol to determine the minimum and maximum dimensional constraint, respectively. These proportions are consistent with the methyl group of methanol having free rotation, while the longer chains of ethanol and *n*-propanol could possess some configurational bias due to the channel constraints.

(78) Helmer, F.; Kiehs, K.; Hansch, C. *Biochemistry* **1968**, *7*, 2858−2863.

(79) Turconi, S.; MacLachlan, D. J.; Bratt, P. J.; Nugent, J. H. A.; Evans, M. C. *Biochemistry* **1997**, *36*, 879−885.

(80) Tang, X.-S.; Sivaraja, M.; Dismukes, G. C. *J. Am. Chem. Soc.* **1993**, *115*, 2382−2389.

(81) Roelofs, T.; Liang, W.; Latimer, M.; Cinco, R.; Rompel, A.; Andrews, J.; Sauer, K.; Yachandra, V.; Klein, M. *Proc. Natl. Acad. Sci. U.S.A.* **1996**, *93*, 3335−3340.

(82) Carrington, A.; McLachlan, A. D. *Introduction to Magnetic Resonance*; Harper & Row: New York, 1967; pp 80−85.

binding at the S_2-state. As stated earlier, an advantage of the approach taken here with deuteration of the nonexchangeable hydrogens of these small alcohols is that there is no ambiguity as to the chemical species binding near the Mn cluster. Therefore, coupled with the detailed ESEEM analysis, we can conclude with a high degree of certainty that the small alcohols are binding directly to the Mn cluster. Given this result, it is difficult to imagine that in the absence of alcohol, given the similarity in binding mode of water and the enormous ~55 M water concentration, that water or hydroxide would not bind in this alcohol binding site. And as stated above, our recent ESEEM and ENDOR studies do provide direct experimental evidence that water or hydroxide binds to the Mn cluster at the S_2-state.

Given that methanol and ethanol can bind to the Mn cluster at the S_2-state, it is interesting that at these $\leq$1.0 M concentrations, there is no inhibition of oxygen evolution activity. One possibility is that the alcohol ligates at a binding site that is distinct from the substrate water-binding sites. It is also possible that the small alcohols can displace water at a common binding site at the S_2-state, midway around the Kok cycle, but that alcohol can be displaced by 55 M water at the highly oxidized S_4-state where final water oxidation occurs. This would be consistent with the hard−soft acid−base (HSAB) concept that the harder, more oxidized S_4-state of the cluster would preferentially bind the harder water ligand. Alternatively, both water and alcohol may bind at S_4 in rapid equilibrium, with the exchange kinetics sufficiently fast that exchange of water into the site provides no kinetic bottleneck to water oxidation. Further experiments are required to distinguish between these various possibilities.

In terms of S-state dependencies to the alcohol binding properties, the facts that methanol and ethanol deuteron couplings are observed in samples advanced to the S_2-state via low-temperature (200 K) illumination and that no appreciable changes are observed in the "annealing" step undertaken to allow for rapid ligand exchange are strongly suggestive that the alcohols are already bound at the S_1-state (see Boussac et al.[54]). Moreover, the fact that methanol is required to observe the newly reported S_0 multiline signal[26−28] suggests that it may ligate even at this most reduced state of the Kok cycle.

Acknowledgment. A grant from the National Institutes of Health (GM48242) is gratefully acknowledged by R.D.B.

Appendix: Description of Numerical Methods

Theoretical Background. The dipolar hyperfine interaction of a proton with an exchange-coupled multinuclear metal ion complex is the sum of the individual effective dipolar hyperfine interactions:[66,67]

$$\tilde{\mathbf{A}}_{\mathrm{dip}}^{\mathrm{Total}} = \sum_i p_i \tilde{A}_{\mathrm{dip},i} \qquad (1)$$

where i is the index of the Mn ions and an effective dipolar hyperfine interaction is the product $p_i \tilde{A}_{\mathrm{dip},i}$, where the p_i terms are the quantum mechanical projection factors for each Mn ion and $\tilde{A}_{\mathrm{dip},i}$ is the point dipolar hyperfine interaction matrix between the proton and Mn ion i. For the Mn cluster of the OEC, we use projection factors determined by spectral simulations of the multiline EPR spectrum by Zheng and Dismukes.[73] These Mn projection factors are $^5/_3$, $^5/_3$, $-^4/_3$, and -1 for a ferromagnetically exchange-coupled Mn(III)−Mn(III) moiety antiferromagnetically exchange-coupled to a second ferromagnetically exchange-coupled Mn(III)−Mn(IV) moiety.[73] This $Mn(III)_3Mn(IV)$ oxidation state model for the S_2-state is different than the $M(III)Mn(IV)_3$ XANES (X-ray absorption near edge structure)-derived S_2−state assignment for the cluster.[81] However, the approximate projection factors for several other spin states, including the $Mn(III)Mn(IV)_3$, are roughly similar to those of this Mn oxidation state model (see Zheng and Dismukes,[73] especially the supplementary material). Consequently, the qualitative trends of the calculations presented here are valid, independent of oxidation/spin state assignment.

The summation in eq 1 must be performed in a common axis system.[40,66] In the case of the dinuclear cluster, a common axis system was chosen where the z-axis fell along the Mn−Mn axis and the y-axis was normal to the Mn(III)−Mn(IV)−H plane. For tetranuclear clusters, which can occur in a variety of arrangements, such symmetry will not generally exist. Therefore, an arbitrary axis system may be used and for convenience we use an axis system that defines the cluster itself (i.e., the axis system in which the coordinates of the Mn atoms are expressed). In this axis system each dipolar hyperfine interaction matrix, $\tilde{A}_{\mathrm{dip},i}$, in eq 1 is given by[82]

$$\tilde{A}_{\mathrm{dip},i} = -\frac{g_e g_N \beta_e \beta_N}{r_i^5}\begin{bmatrix} r_i^2 - 3x^2 & -3xy & -3xz \\ -3xy & r_i^2 - 3y^2 & -3yz \\ -3xz & -3xy & r_i^2 - 3z^2 \end{bmatrix} \qquad (2)$$

where x, y, and z are the coordinates of the proton and r_i is the distance from Mn atom i to the proton defined as follows:

$$r_i = |\vec{x} - \vec{x}_{\mathrm{Mn},i}| = \sqrt{(x - x_{\mathrm{Mn},i})^2 + (y - y_{\mathrm{Mn},i})^2 + (z - z_{\mathrm{Mn},i})^2} \qquad (3)$$

where $\vec{x} = (x, y, z)$ and $\vec{x}_{\mathrm{Mn},i}$ is an analogous vector whose elements are the coordinates of Mn ion i.

All terms in the summation in eq 1 have now been defined, and the summation can be performed. Diagonalizing the resulting symmetric dipolar hyperfine interaction matrix yields the principal components of the dipolar hyperfine tensor. Unfortunately, in practice the diagonalization is virtually impossible to perform analytically since no symmetry exists for a general tetranuclear cluster. Hence numerical methods are required.

Implementation of Numerical Methods. Numerical methods are used to evaluate the components of the dipolar hyperfine interaction of a "test proton" at specified points in the space surrounding the Mn cluster. We start by evenly dividing the space surrounding the Mn cluster into a three-dimensional grid. At each point where three orthogonal grid lines intersect, we calculate the total undiagonalized dipolar hyperfine interaction ($\mathbf{A}_{\mathrm{dip}}^{\mathrm{Total}}$) for a "test proton" as described above in eq 1. The resulting 3 × 3 matrix is symmetric, and a numerical diagonalization procedure (vide infra) facilely determines its eigenvalues which are the principal components of the dipolar

(83) The matrix diagonalization routines are not part of the standard Igor package (version 3.0) and were ported to Igor by David Niles at the National Renewable Energy Laboratories based on routines from *Numerical Recipies in C*.

(84) Sauer, K.; Yachandra, V. K.; Britt, R. D.; Klein, M. P. In *Manganese Redox Enzymes*; Pecoraro, V. L., Ed.; VCH: New York, 1992; pp 141−174.

(85) Derose, V. J.; Mukerji, I.; Latimer, M. J.; Yachandra, V. K.; Sauer, K.; Klein, M. P. *J. Am. Chem. Soc.* **1994**, *116*, 5239−5249.

(86) Penner-Hahn, J. E.; Fronko, R. M.; Pecoraro, V.; Yocum, C. F.; Betts, S. D.; Bowlby, N. R. *J. Am. Chem. Soc.* **1990**, *112*, 2549−2557.

(87) George, G. N.; Prince, R. C.; Cramer, S. P. *Science* **1989**, *243*, 789−791.

hyperfine interaction. Each eigenvalue (hyperfine component) is stored in a separate three-dimensional array, whose dimensions are the number of points in the *x*, *y*, and *z* directions into which the Mn cluster has been placed. The entire procedure was written as an [internal] function using Igor software (Wavemetrics, Lake Oswego, OR).[83]

Computational Results. For the calculations, Mn cluster arrangements based on a dimer-of-dimers model,[70] cubane structure,[72] and butterfly arrangement[71] were used (Scheme 1). Of the models considered here, only the Berkeley model for the Mn ion arrangement has Mn−Mn distances of 2.7 and 3.3 Å, which are supported by EXAFS (extended X-ray absorption fine structure) experiments.[70,84,85] Though the 3.3 Å distance is attributed by these workers to a Mn−Mn backscattering interaction, this assignment remains open.[86,87] As argued in Randall et al.,[40] the middle-valued component of the dipolar hyperfine interaction tensor (A_{mid}) gives the most intense ENDOR feature and is therefore most likely to influence the spectrum regardless of the degree of rhombicity, $\chi = |(A_{min} - A_{mid})|/A_{max}$. Here, A_{min} is the smallest component of the dipolar hyperfine interaction and A_{max} the largest component. Interpolated isosurfaces, where the A_{mid} component of the dipolar hyperfine interaction is constant, were obtained using the program DataExplorer.[42]

JA982713B